Geol. Mag. **148** (3), 2011, pp. 423–434. © Cambridge University Press 2010
doi:10.1017/S0016756810000841

Formation of spinel-cordierite-plagioclase symplectites replacing andalusite in metapelitic migmatites of the Alvand aureole, Iran

A. SAKI*

Department of Geology, Faculty of Science, Shahid Chamran University, Ahvaz, 65355-141, Iran

(*Received* 4 January 2010; *accepted* 4 August 2010; *first published online* 22 October 2010)

Abstract – Spinel–cordierite–plagioclase symplectites partially replacing andalusite occur in the metapelitic migmatite rocks of the Alvand aureole within the Sanandaj–Sirjan metamorphic belt, Hamadan, Iran. The presence of melt shows that corona development occurred under partial melting conditions. Spinel is predicted to grow with cordierite at around 700 °C. Exhaustion of the available SiO_2 and/or separation of sillimanite/andalusite from SiO_2-rich matrix domains by cordierite resulted in the formation of localized low-silica activity domains and thus triggered the growth of spinel in the rim of andalusite, the reaction Sil/And + Bt = Crd + Spl + Kfs + melt, as the most common reaction for the development of coronas in the metapelitic of Alvand aureole. The breakdown of garnet to plagioclase + sillimanite, dehydration melting and the formation of spinel–plagioclase symplectite could occur during heating or decompression; these textures are limited to the contact aureole in the studied area, so heating is perhaps the more likely explanation for formation of the symplectites in the metapelitic rocks of the Alvand aureole. The *P–T* diagram, inferred paths and zoning profiles of garnet do not account for the decompression history of the terrane.

Keywords: spinel–cordierite–plagioclase symplectites, Alvand aureole, *P–T* diagram, dehydration melting, decompression.

1. Introduction

The mineral assemblage garnet–spinel–cordierite–feldspar–quartz–biotite–sillimanite is typical of metapelitic systems at high temperature (HT) and low (LP) to medium pressure (MP) (e.g. Hand *et al.* 1994; McDade & Harley, 2001; White, Powell & Holland, 2001; White, Powell & Clarke, 2002; Cenki, Kriegsman & Braun, 2002; Ings & Owen, 2002; Riesco *et al.* 2004). Such *P–T* conditions are also propitious for the assemblage to be accompanied by melt, derived by partial melting of the rocks. A typical microstructural feature in these metapelites is the intergrowth of spinel and cordierite, which usually replaces garnet–sillimanite-bearing assemblages (e.g. Mezger, Chacko & Erdmer, 2001; Topuz *et al.* 2004), and/or andalusite (Cesare *et al.* 2003; Johnson *et al.* 2004). Symplectites of spinel and cordierite replacing andalusite and/or sillimanite have been reported from many high-temperature regional metamorphic terranes and several contact aureoles, and commonly these symplectites are inferred to record decompression with reaction occurring within restricted silica-deficient compositional domains focused around aluminosilicate (e.g. Bucher-Nurminen & Droop, 1983; Droop, 1989; Grant & Frost, 1990; Clarke & Powell, 1991; Waters, 1991; Carson *et al.* 1997; Greenfield, Clarke & White, 1998; Pitra & de Waal, 2001; Norlander *et al.* 2002; White, Powell & Clarke, 2003). Spinel–cordierite assemblages may occur as coronitic and/or symplectite microstructures, related to particular kinetic conditions of a low chemical diffusion rate (Hand *et al.* 1992; Passchier & Trouw, 1996; Vernon, 1996; Whittington, Harris & Baker, 1998). The presence of such symplectites and the correct interpretation of their petrogenesis have consequences for understanding the tectonothermal evolution of segments of the crust, and in investigating equilibration volumes and diffusion-controlled fractionated domainal bulk compositions (e.g. Stüwe, 1997; Marmo, Clarke & Powell, 2002). Spinel–cordierite symplectites replacing andalusite are found locally in metapelites within the migmatite rocks in the Alvand aureole. However, the occurrence of such symplectites within the aureole of the Alvand Complex, and the absence of such symplectites within regional metamorphic rocks elsewhere in the Hamadan area, raises doubts about the general applicability of this model. In this paper, we investigate in detail migmatized andalusite- and symplectite-bearing metapelitic rocks from the Alvand aureole within the Sanandaj–Sirjan metamorphic belt, Hamadan.

2. Geological setting

The study area is a part of the 1500 km long Sanandaj–Sirjan metamorphic belt of the Zagros orogen of western Iran (Fig. 1a, b). The Zagros formed during subduction of a Neo-Tethyan seaway and subsequent oblique collision of Afro-Arabia (Gondwana) with the Iranian microcontinent in Late Cretaceous–early Tertiary times (Berberian & King, 1981; Alavi, 1994; Mohajjel & Fergusson, 2000). Crustal shortening associated with subduction and collision metamorphosed and deformed Late Palaeozoic and Mesozoic

*E-mail: adel_saki@scu.ac.ir or adel_saki@yahoo.com

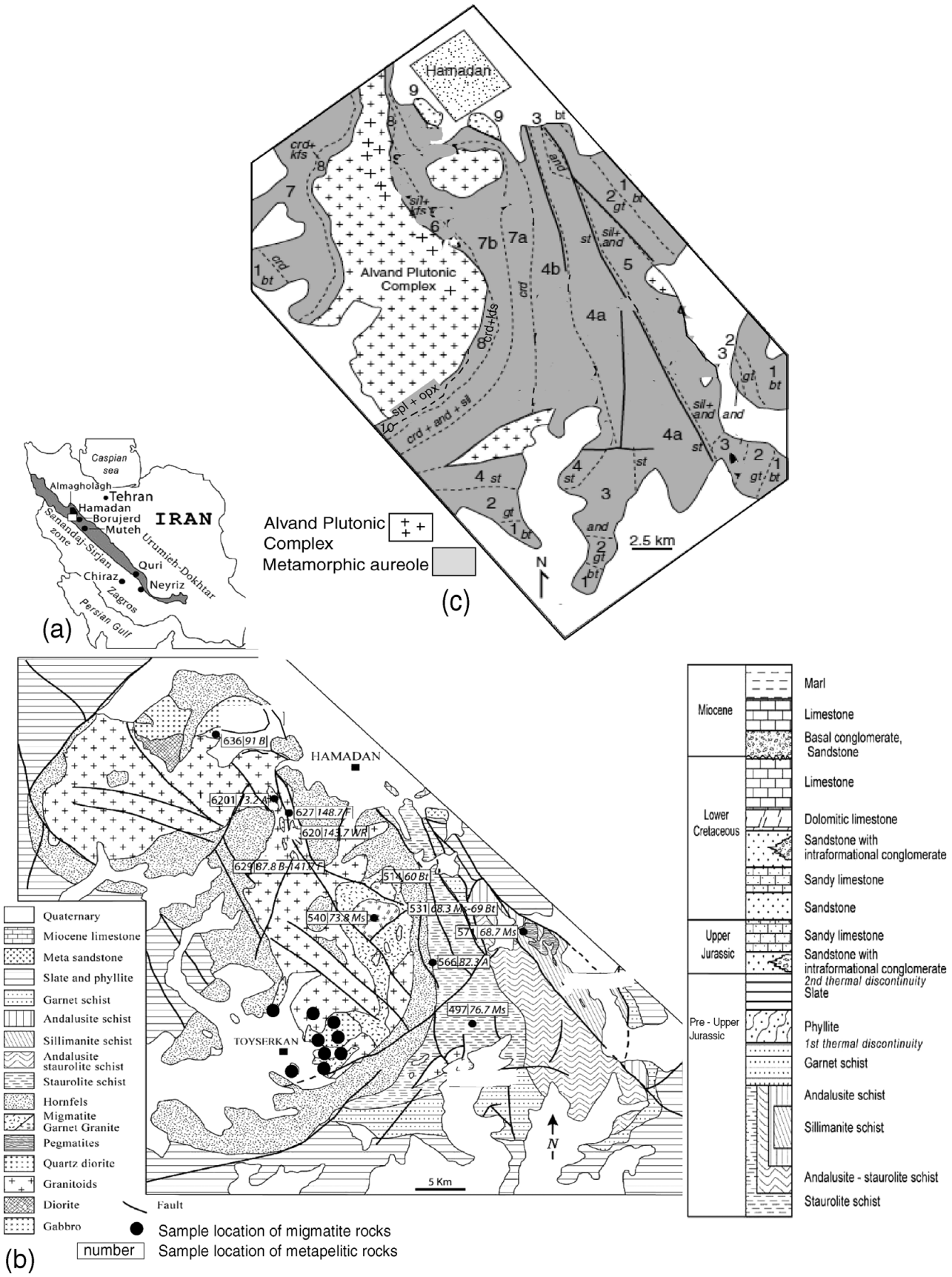

Figure 1. (a) Location of the Sanandaj–Sirjan belt in Iran. (b) Geological map of the area (modified from Baharifar *et al.* 2004), with sample locations and stratigraphic column of the area. (c) Generalized geological map of the study area near Hamadan. Isograds (dashed lines) and metamorphic zones are shown (modified from Sepahi, Whitney & Baharifar, 2004). Some faults are shown (heavy lines within unit 4); contacts between zones 4a–4b, 4a–5, 2–5, and possibly 4–7 are faults. Zones: 1 – biotite zone; 2 – garnet zone; 3 – andalusite zone (±fibrolite); 4 – staurolite zone (a = staurolite + andalusite ± fibrolite; b = staurolite + garnet, no andalusite); 5 – sillimanite–andalusite zone; 6 – sillimanite–Kfs zone; 7 – cordierite zone (a = cordierite with no new growth of Al_2SiO_5; b = cordierite + neoblastic andalusite + sillimanite); 8 – cordierite Kfs zone; 9 – spotted schist; 10 – spinel + orthopyroxene zone (migmatites).

https://doi.org/10.1017/S0016756810000841 Published online by Cambridge University Press

sedimentary rocks, including a sequence of pelitic, psammitic, mafic, calc-pelitic and calc-silicate rocks near Hamadan (Fig. 1b).

During the Palaeozoic period, the Sanandaj–Sirjan Zone (SSZ) was part of northeast Gondwanaland, separated from the Eurasian plate by the Palaeo-Tethys ocean (Golonka, 2004; Sears, George & Winne, 2005; Shahabpour, 2005, Ahmadi *et al.* 2007; Fazlnia *et al.* 2009). From early Permian to early Triassic times, the SSZ was situated along the southern margin of the Eurasian plate, separated from northern Gondwanaland by the Neo-Tethyan ocean (Mohajjel, Fergusson & Sahandi, 2003; Khalaji *et al.* 2007; Fazlnia *et al.* 2009). During the Mesozoic, the oceanic crust of the Neo-Tethys was subducted beneath the Eurasian plate (Mohajjel, Fergusson & Sahandi, 2003; Golonka, 2004; Shahabpour, 2005; Ahmadi *et al.* 2007; Fazlnia *et al.* 2009), and the SSZ occupied the position of a magmatic arc (Berberian & Berberian, 1981; Arvin *et al.* 2007). The final closure of the Neo-Tethys and the collision of the Arabian and Eurasian plates took place during the Tertiary period (Berberian & Berberian, 1981), and during the same period, the Zagros Fold and Thrust Belt formed as part of the Alpine–Himalayan mountain chain, extending to about 2000 km from eastern Turkey to the Oman line in southern Iran (Agard *et al.* 2005; Mohajjel, Fergusson & Sahandi, 2003; Ahmadi *et al.* 2007; Omrani *et al.* 2008).

The Sanandaj–Sirjan zone contains abundant Mesozoic arc-related plutonic and plutono-metamorphic complexes, such as Alvand, Almogholagh, Samen, Ghorveh, Borojerd, Urumieh, Arak, Astaneh, Qori and Siah-Kuh.

The U–Pb dating results demonstrate that all granitoids were exclusively emplaced during the Jurassic period instead of being Cretaceous or younger in age as suggested previously (Shahbazi *et al.* 2010). The pluton was assembled incrementally over about 10 Ma. Gabbros formed at 166.5 ± 1.8 Ma, granites between 163.9 ± 0.9 Ma and 161.7 ± 0.6 Ma, and leucocratic granitoids between 154.4 ± 1.3 and 153.3 ± 2.7 Ma. Granites and leucocratic granitoids show some A-type affinity. It is concluded that the Alvand plutonic complex was generated in a continental-arc-related extensional regime during subduction of Neo-Tethyan oceanic crust beneath the SSZ (Shahbazi *et al.* 2010).

The tectonic evolution of the Sanandaj–Sirjan belt involved continental arc magmatism followed by collision. Mafic to intermediate plutonic bodies (olivine gabbro, gabbro, gabbro-norite, diorite, quartz diorite and tonalite) are older than crustally derived granitic plutons in the region (Alvand Plutonic Complex). All metamorphic rocks in the area that were regionally metamorphosed prior to the contact metamorphism up to greenschist to amphibolite facies underwent contact metamorphism due to emplacement of the Alvand Complex. The plutons, including the granites, are commonly associated with contact aureoles defined by migmatites, hornfelsic textures and mineral assemblages that overprint earlier minerals and fabrics. Migmatitic rocks are located in the southwestern part of the Alvand Complex near the city of Toyserkan (Fig. 1b).

3. Field observations

In the field area near Hamadan, igneous and metapelitic rocks are the most abundant rock type and are interlayered with minor metabasaltic rocks (amphibole schist and amphibolite), metacarbonates and calc-silicate rocks.

Calc-silicate rocks have formed in the eastern part of this batholite. The peak metamorphic assemblage of calc-silicate rocks is garnet, diopside, vesuvinite, wollastonite and calcite. *P–T* results indicate that a contact metamorphism condition occurs in pyroxene hornfels facies in this part of the Hamadan crust (Saki & Pourkaseb, 2010).

Critical metamorphic mineral assemblages in the metapelitic rocks indicate regional metamorphism under amphibolite-facies conditions. The dominant metamorphic assemblage of regional metapelitic rocks is Ms + Bt + Grt + St + And + Sil/Ky.

Contact metamorphism overprinted the older regional metamorphic assemblages. The main peak contact metamorphic assemblage is Grt + Bt+ And + Ms + Sil + Crd + Spl ± Opx.

Metapelitic rocks occur as slate, phyllite, mica schist, garnet schist, garnet–andalusite (±sillimanite or kyanite) schist, garnet–staurolite schist and garnet–sillimanite (±kyanite) schist, hornfelsic and migmatitic rocks (near the Alvand Plutonic Complex). These contact zone rocks include cordierite + K-feldspar (±andalusite, fibrolite) and garnet–staurolite (±kyanite) hornfels. In the Hamadan metamorphic sequence, cordierite and K-feldspar are only found near (< 3 km from) the Alvand granite. The general trend of increasing metamorphic grade is towards the pluton, with a succession of isograds in metapelitic rocks: biotite-in, garnet-in, andalusite-in, staurolite-in, cordierite-in, K-feldspar-in and spinel-in. In some parts of the field area, the complete sequence occurs, but in other areas, some of the lower grade zones are missing (Fig. 1c).

Faulting has disrupted the sequences in places, and some apparent isograds may actually be faults. The most obvious example of disruption of the sequence by faulting is the fault-bounded panel of andalusite–sillimanite schists (zone 5) that occurs between the andalusite and staurolite zones (Fig. 1c).

As mentioned above, pelitic rocks, containing pale quartz-feldspar (granitoid) veins, appear in the upper Spinel Zone and Sillimanite Zone. Because these rocks are mixed rocks with quartz-feldspathic parts (leucosomes) and darker coloured parts, more enriched in ferromagnesian minerals, we will use the term ‘migmatite’ (Sederholm, 1967) for them.

The migmatites are best developed on the southern side of the Alvand complex (Fig. 2). Migmatitic metamorphic zones occur at several localities that are

https://doi.org/10.1017/S0016756810000841 Published online by Cambridge University Press

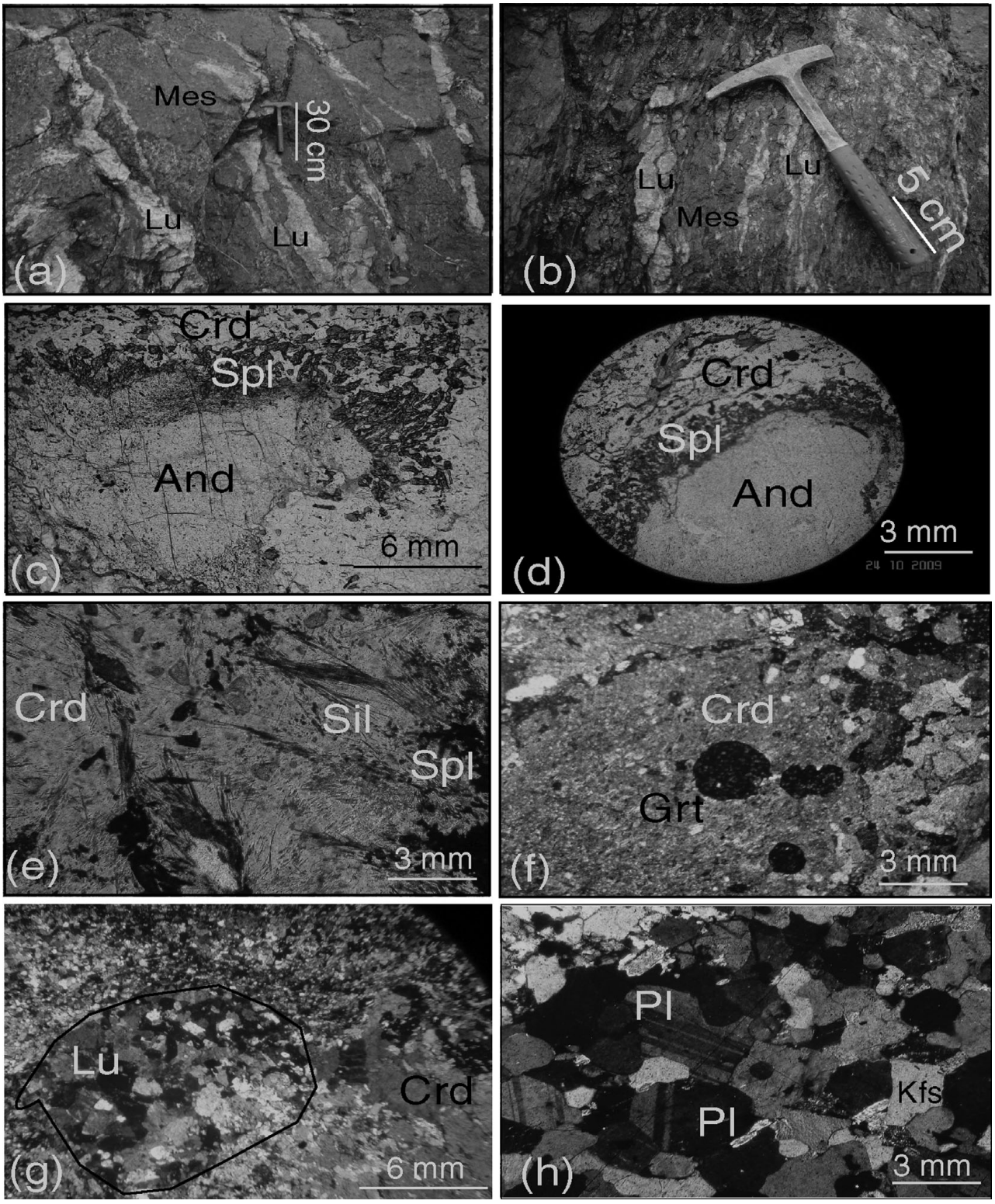

Figure 2. Field photographs of migmatites. A colour version of this figure is available at http://www.cambridge.org/journals/geo. (a, b) Migmatite in which smaller leucosomes in (a) and (b) appear to be crystallized from melt derived locally, whereas the larger leucosome likely records evidence of melt moving through the system. (c, d) Plane-polarized light view of a Spl + Crd + And corona in the mesosome. (e) Sil + Crd + Spl in the mesosome. (f) The garnet as inclusion in the cordierite. (g) Feldspar–plagioclase–quartz patches (Lu), with the melt apparently segregated into mesoscopic patches or veins. (h) Euhedral shape of the plagioclase phenocrysts against intersertal quartz in (g).

in close proximity to batholithic contacts within the Alvand aureole pelites of the Hamadan region (Saki, Moazzen & Baharifar, unpub. data). The migmatite zone shown in Figure 1c is the most extensive of these and can be related to a very well-defined metamorphic gradient through the metapelite unit.

The leucosomes that developed during migmatization can be morphologically divided into: (1)

https://doi.org/10.1017/S0016756810000841 Published online by Cambridge University Press

concordant (stromatitic) and pervasive network leucosomes (Fig. 2a), (2) discordant dykes and pockets of pegmatites and aplites (Fig. 2b), and (3) agmatitic and randomly distributed leucosome patches of various sizes, which appear to represent the gathering of quartzo-feldspathic segregations into larger, granitic or pegmatitic tubes and dykes.

4. Petrography

Petrographic characteristics of the symplectite-bearing rocks are based on observations of several samples. The rocks are composed of three mesoscopic components: a cordierite-, K-feldspar, andalusite and biotite-rich matrix (mesosome); partial pseudomorphs in which resorbed andalusite is surrounded by spinel–cordierite symplectites; quartz-, K-feldspar- and/or plagioclase-rich leucosome that commonly shows a close spatial relationship with the pseudomorphs but which also occurs as pockets within the matrix.

4.a. Mesosomes

Mesosomes in patches and stromatic migmatites (patch migmatites formed by *in situ* melting) are massive (Fig. 2a, b). The matrix (mesosomes) contains cordierite, K-feldspar, biotite, andalusite and quartz with minor plagioclase, garnet and ilmenite. Cordierite forms randomly oriented subhedral grains up to 10 mm in length and has garnet inclusions (Fig. 2f). At least two microstructural variants of cordierite occur in these samples: (1) cordierite as a constituent of the coronas around andalusite (Fig. 2c, d); (2) cordierite crystals in the matrix, with inclusions of melt, biotite and sillimanite (Fig. 2e). Andalusites have equidimensional shape and resorbed rims, and are generally < 20 mm in length. Locally, spinel has a thin rim of plagioclase. K-feldspar forms anhedral grains up to 2 mm across; cores are riddled with finely disseminated opaque inclusions and larger inclusions of quartz and biotite and exhibit a micro-perthitic microstructure.

4.b. Leucosomes

Migmatites in the Alvand aureole exhibit different leucosome shapes. The leucosomes exhibit mesoscopic (Fig. 2a, b) to microscopic (Fig. 2g) structure, are fine- to coarse-grained and show magmatic texture (Fig. 2h). They are leucotonalitic to granitic in composition, as some strings and layers consist of distinct portions that are either rich in Kfs or in Pl or are made up of Qtz + Grt + two feldspars. This seems to indicate that melt segregation was not completely efficient and that melt did not migrate over long distances; some migration did occur, however, as indicated by the discordant and concordant leucosomes and by the variable concentration of leucosomes at outcrop scale. Leucosomes are composed of quartz, plagioclase and K-feldspar in different proportions. Pl may be the only feldspar in some leucotonalitic types; Kfs exceeds 50 vol. % within some granitic bodies; Qtz, independently of the composition of the rocks, may exceed 60 vol. %. Garnet is present in leucosomes as coarse crystals up to 1 cm in diameter. The granitic bodies associated with metapelites are composed of large subhedral and embayed crystals of Kfs, more rarely Pl with interstitial fine- to medium-grained Qtz, Pl and Kfs and large euhedral crystals of garnet. Leucosomes preserve textures resulting from the presence of melt, such as euhedral phenocrysts/peritectic phases, textures that mimic solid–melt relations (quartz/feldspar films along grain boundaries, interstitial–xenomorphic quartz, and residual quartz in feldspar), melt–solid reaction textures and fractured residual grains (Saki & Baharifar, 2010).

4.c. Pseudomorphs

The partial pseudomorphs of andalusite are up to 10 mm long and make up 5–10 vol. % of the rock. They comprise a variably resorbed andalusite surrounded by a rim of symplectite composed of spinel, cordierite and plagioclase that may be in excess of 1 mm wide (Fig. 2e, f). The symplectites are surrounded by a moat of pure cordierite, up to 1 mm wide, in which individual stubby cordierite grains are aligned perpendicular to the symplectite–andalusite interface. The symplectite rim and cordierite moat are surrounded by K-feldspar- and/or plagioclase-rich, quartz-poor leucosomes and/or by a coarse-grained biotite fringe that grades into K-feldspar-poor matrix (Fig. 2g, h).

4.d. Corona microstructure

The corona microstructure is composed of a partly to completely resorbed andalusite up to 20 mm in diameter which shows a corona of Spl + Crd + Pl that is only present between andalusite and the matrix. The corona displays a shell of subhedral spinel within a matrix of cordierite, K-feldspar and plagioclase. Spinel is in contact with the matrix or with andalusite (Fig. 2c, d). In a few cases, spinel in the corona shows a thin rim of plagioclase. The melt was present throughout the history of the andalusite formation and its subsequent partial replacement by coronitic phases.

5. Mineralogy

Major element compositions of biotite, garnet, spinel, plagioclase, cordierite and ilmenite in selected samples (migmatite rocks) were determined by wavelength-dispersive spectrometry using a Cameca SX100 microprobe. The operational conditions were 15 kV, 10–20 nA specimen current. The analytical spot diameter was set between 3 and 5 μm, keeping the same current conditions. Natural and synthetic standards were used for calibration. Ferric iron contents in ferromagnesian minerals are calculated using stoichiometric criteria (Droop, 1989). Mineral abbreviations are from Kretz (1983).

https://doi.org/10.1017/S0016756810000841 Published online by Cambridge University Press

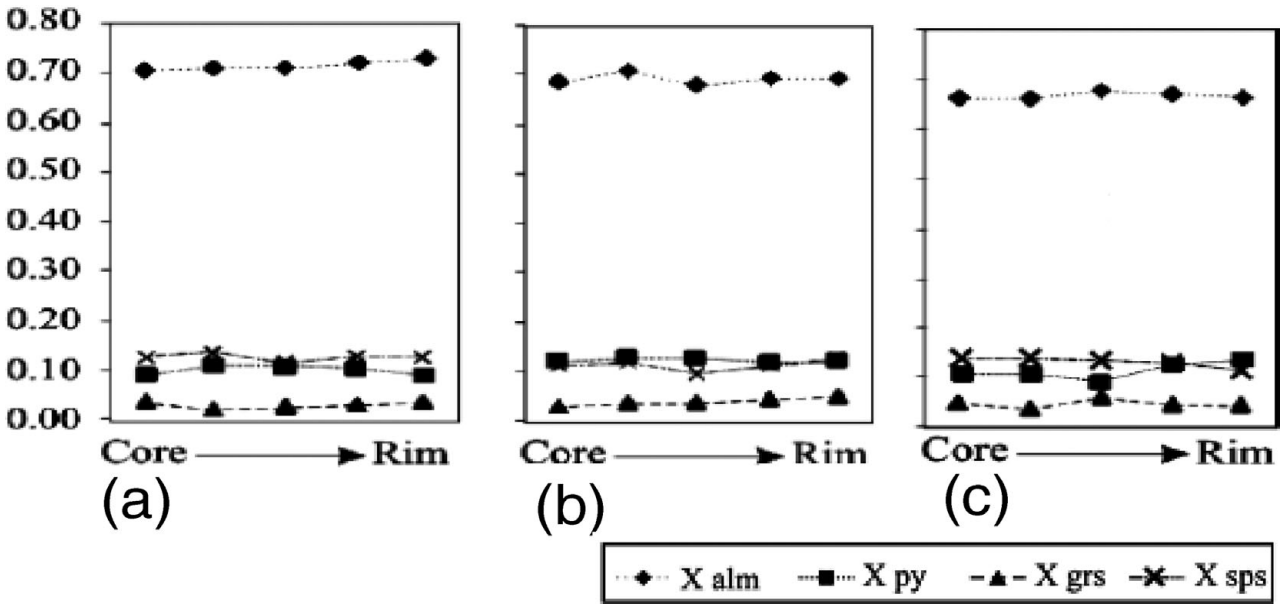

Figure 3. Zoning profile from core to rim through the garnet in some samples of migmatite (mesosome; contact metamorphism), which shows a flat profile attributed to garnet crystallization in these rocks.

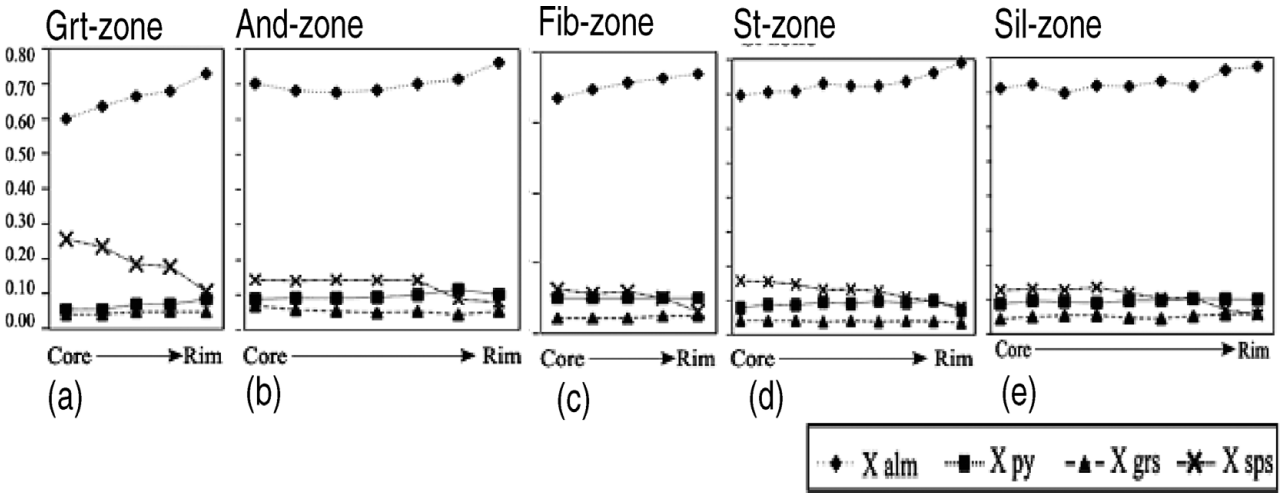

Figure 4. Zoning profile of the garnet in some samples from the regional metapelitic rocks, which shows prograde metamorphism (normal zoning) attributed to garnet crystallization in different regional metamorphic zones.

5.a. Garnet

Garnet compositions are listed in Table 1. In general, garnets are Fe-rich, with almandine content varying between 80 and 90 %. Ti is not presented or occurs in very small amounts. Figure 3 shows the flat zoning profiles of garnet in the migmatite rocks (contact metamorphic rocks). Zoning profiles are from core to rim of the contact and regional garnets (Fig. 4).

The pronounced normal zoning in the regional metamorphic garnet from some samples can be seen in Figure 4.

5.b. Cordierite

Cordierite compositions are listed in Table 1. The average EMP total of cordierite is > 98.5. In the K-feldspar–cordierite, sillimanite–K-feldspar and spinel–cordierite zones, cordierite is homogeneous in thin-section. Cordierite in the muscovite–cordierite zone is completely pinitized. X_{Mg} of cordierite shows no systematic change with ascending metamorphic grade from the K-feldspar–cordierite zone to the spinel–cordierite zone (0.45–0.62).

5.c. Biotite

Table 2 includes the microprobe analyses of biotite in the studied samples. Biotite has high TiO_2 contents, ranging from 3.02 to 3.25 wt %. Phlogopite–annite is the dominant constituent in the biotite. Classification after Robinson *et al.* (1982) indicates that peak metamorphism biotite belongs to the Sil–Kfs and Grt–Crd–Kfs zone type.

5.d. Spinel

Spinel compositions are listed in Table 2. This is a hercynite-rich solid solution that has compositions in the range $X_{(Her)}$ 0.86–0.89.

https://doi.org/10.1017/S0016756810000841 Published online by Cambridge University Press

Table 1. Representative mineral analyses of garnet and cordierite

Sample	Tu1	Tu1	Tu1	Tu1	Tu1	Tu1	Tu1	Tu1	Tu1	Tu1	Tu1	Tu1	Tu1
Mineral	Grt (Rim)	Grt (Cor)	Grt (Cor)	Grt (Rim)	Grt (Rim)	Grt (Rim)	Grt (Rim)	Grt (Rim)	Crd	Crd	Crd	Crd	Crd
SiO_2	36.84	36.82	36.68	36.16	36.85	37.36	37.63	37.10	48.07	47.98	48.09	48.42	48.42
TiO_2	0.02	0.03	0.00	0.00	0.00	0.04	0.00	0.00	0.00	0.00	0.01	0.01	0.06
Al_2O_3	20.98	20.71	21.00	21.63	20.77	20.93	21.06	20.97	32.53	32.35	32.29	32.92	32.60
Cr_2O_3	0.00	0.00	0.01	0.04	0.10	0.12	0.08	0.00	0.00	0.00	0.05	0.00	0.00
Fe_2O_3	0.86	1.46	1.07	2.19	1.83	0.27	0.54	1.09	1.75	0.68	1.26	1.17	0.61
FeO	34.93	31.33	31.16	34.35	35.22	32.99	32.78	31.79	8.64	9.74	9.35	9.00	9.19
MnO	3.70	4.75	4.83	3.39	3.81	6.42	5.03	4.87	0.55	0.70	0.60	0.45	0.55
MgO	2.39	3.32	3.26	2.65	2.43	2.17	3.06	3.33	7.14	6.52	6.58	7.11	7.06
CaO	0.67	1.56	1.56	0.57	0.51	1.06	1.19	1.22	0.01	0.02	0.06	0.04	0.01
Na_2O	0.00	0.00	0.00	0.00	0.00	0.00	0.03	0.00	0.18	0.19	0.16	0.18	0.19
K_2O	0.00	0.00	0.00	0.00	0.01	0.00	0.00	0.00	0.00	0.00	0.16	0.00	0.01
Total	98.60	99.83	99.45	100.75	101.52	101.32	101.35	100.29	98.70	98.11	98.48	99.17	98.65
				Cations per 12 oxygen atoms						*Cations per 18 oxygen atoms*			
Si	2.998	2.970	2.967	2.909	2.959	2.997	2.996	2.978	4.968	5.004	4.997	4.978	5.006
Ti	0.012	0.002	0.000	0.000	0.000	0.002	0.000	0.000	0.000	0.000	0.001	0.001	0.005
Al	2.032	1.969	2.002	0.000	1.965	1.978	1.976	1.984	3.963	3.977	3.955	3.989	3.972
Cr	0.000	0.000	0.000	2.050	0.006	0.008	0.005	0.000	0.000	0.000	0.004	0.000	0.000
$Fe^{(3+)}$	0.053	0.089	0.065	0.132	0.111	0.016	0.032	0.066	0.136	0.053	0.098	0.091	0.047
$Fe^{(2+)}$	2.401	2.113	2.107	2.311	2.365	2.213	2.183	2.134	0.747	0.850	0.812	0.773	0.794
Mn	0.258	0.324	0.331	0.231	0.259	0.435	0.339	0.331	0.048	0.062	0.053	0.039	0.048
Mg	0.293	0.399	0.393	0.318	0.291	0.259	0.363	0.398	1.100	1.014	1.019	1.090	1.088
Ca	0.059	0.135	0.135	0.049	0.044	0.91	0.102	0.105	0.001	0.002	0.007	0.004	0.001
Na	0.000	0.000	0.000	0.000	0.000	0.000	0.005	0.005	0.036	0.038	0.032	0.036	0.038
K	0.000	0.000	0.000	0.000	0.000	0.000	0.000	0.000	0.000	0.000	0.021	0.000	0.001
Total	8.000	8.000	8.000	8.000	8.000	8.000	8.000	8.000	11.00	11.00	11.00	11.00	11.00
$Mg/(Mg+Fe_2)$	0.109	0.159	0.157	0.121	0.110	0.105	0.143	0.157					
$Fe_2/(Fe_{tot})$	1.023	0.960	0.970	0.946	0.955	0.993	0.985	0.970					

Fe^{2+}/Fe^{3+} ratio in garnet is calculated using stoichiometry.

Table 2. Representative mineral analyses of biotite, spinel and ilmenite

Sample	Tu1	Tu1	Tu1	Tu		Tu1	Tu	Tu1	Tu	Tu1
Mineral	Bt	Bt	Bt	Bt		Spl	Spl	Spl	Ilm	Ilm
SiO_2	35.45	35.45	35.20	35.30		0.00	0.00	0.02	0.00	0.02
TiO_2	3.02	3.10	3.20	3.25		0.00	0.00	0.00	52.82	54.44
Al_2O_3	17.63	17.95	17.93	18.24		58.48	58.14	57.03	0.03	0.02
P_2O_5	0.02	0.04	0.00	0.00		0.08	0.00	0.06	0.07	0.00
Cr_2O_3	0.12	0.00	0.06	0.03		36.20	36.52	36.79	45.88	43.47
FeO	20.51	21.30	20.80	21.24		1.92	2.95	1.88		
MnO	0.15	0.18	0.11	0.00		0.68	0.72	0.59	2.05	2.01
MgO	9.34	8.09	8.30	8.55		2.93	2.83	2.06	0.10	0.19
CaO	0.00	0.00	0.00	0.00		0.12	0.02	0.00	0.00	0.00
Na_2O	0.11	0.06	0.11	0.10		0.00	0.02	0.05	0.00	0.06
K_2O	9.54	9.74	9.98	10.02		0.00	0.02	0.00	0.00	0.00
Total	95.87	95.87	95.63	96.710		100.22	101.17	98.41	100.97	100.22
	Cations per 11 oxygen atoms					*Cations per 4 oxygen atoms*			*Cations per 8 oxygen atoms*	
Si	2.702	2.716	2.703	2.683		0.000	0.000	0.000	0.000	0.000
Ti	0.171	0.179	0.185	0.186		0.000	0.000	0.000	1.002	1.020
Al	1.580	1.621	1.623	1.634		1.967	1.937	1.957	0.001	0.001
Cr	0.000	0.000	0.000	0.000		0.002	0.000	0.001	0.001	0.000
$Fe^{(3+)}$						0.041	0.063	0.041	0.000	0.000
$Fe^{(2+)}$	1.302	1.365	1.336	1.350		0.860	0.863	0.896	0.968	0.919
Mn	0.010	0.012	0.007	0.000		0.016	0.017	0.015	0.058	0.058
Mg	1.060	0.924	0.950	0.970		0.124	0.119	0.089	0.006	0.008
Ca	0.000	0.000	0.000	0.000		0.000	0.000	0.000	0.000	0.000
Na	0.010	0.000	0.000	0.016		0.000	0.000	0.000	0.000	0.000
K	0.931	0.952	0.978	0.971		0.000	0.000	0.000	0.000	0.000
Total	7.800	7.776	7.798	7.808		3.000	3.000	3.000	1.999	1.980
$X_{Mg(M2)}$	0.341	0.298	0.309	0.313	X_{Fe2+}(Hc)	0.860	0.863	0.896		
$X_{Mg(M1)}$	0.380	0.327	0.333	0.343	X_{Mg} (Spl)	0.124	0.119	0.089		
$X_{Al(T2)}$	0.647	0.642	0.648	0.659	X_{Mn}	0.016	0.017	0.015		
$X_{Al(M2)}$	0.145	0.168	0.163	0.158						
$Mg/(Mg+Fe^2)$	0.455	0.404	0.416	0.418						

For biotite, Fe total is considered as Fe^{2+}.

5.e. Ilmenite

This occurs in all the zones as an accessory phase, not only in pelitic but also in siliceous rocks. Electron-microprobe analyses of ilmenite are provided in Table 2; the ilmenites have a rather constant composition, with $X_{Ilm} = 0.93–0.96$. The MgO content is < 2.02 wt % in all the zones.

5.f. Feldspar

Electron-microprobe analyses of feldspar are provided in Table 3. The anorthite content (X_{An}) of plagioclase is variable; for example, Ca/(Na+K+Ca) is 0.33–0.88. The plagioclases are rich in anorthite. Plagioclases with high Ca content are used for barometry (see below).

Table 3. Representative mineral analyses of feldspar

Mineral	Fsp	Fsp	Fsp	Fsp	Fsp	Fsp
Sample	Tu1	Tu1	Tu1	Tu1	Tu1	Tu1
SiO_2	59.94	45.99	46.35	60.39	60.43	60.67
TiO_2	0.03	0.01	0.05	0.07	0.00	0.00
Al_2O_3	25.07	34.56	34.33	25.51	25.14	25.18
Cr_2O_3	0.00	0.00	0.00	0.08	0.00	0.00
FeO	0.05	0.37	0.22	0.25	0.26	0.20
MnO	0.07	0.02	0.00	0.00	0.00	0.09
MgO	0.01	0.00	0.02	0.03	0.00	0.01
CaO	6.98	17.67	17.91	7.14	6.57	6.58
Na_2O	7.75	1.34	1.44	7.57	7.56	7.84
K_2O	0.12	0.00	0.00	0.15	0.15	0.13
Total	100.02	99.96	100.33	101.20	100.12	100.60
	Cations per 8 oxygen atoms					
Si	2.672	2.119	2.128	2.663	2.686	2.685
Ti	0.001	0.000	0.002	0.002	0.000	0.000
Al	1.317	1.876	1.857	1.326	1.317	1.313
Cr	0.000	0.000	0.000	0.003	0.000	0.000
$Fe^{(3+)}$	0.000	0.000	0.000	0.000	0.000	0.000
$Fe^{(2+)}$	0.002	0.014	0.008	0.010	0.010	0.007
Mn	0.003	0.001	0.000	0.000	0.000	0.003
Mg	0.001	0.000	0.002	0.002	0.000	0.001
Ca	0.333	0.872	0.881	0.337	0.313	0.312
Na	0.670	0.120	0.128	0.647	0.651	0.673
K	0.007	0.000	0.000	0.008	0.009	0.001
Total	5.006	5.003	5.000	4.998	4.986	4.995
Ca/(Na+K+Ca)	0.330	0.879	0.873	0.340	0.322	0.316

6. Conventional geothermobarometry

The Hamadan metamorphic rocks have experienced multiple episodes of metamorphism driven by burial and heating during arc construction and collision, and these events are associated with local partial melting (at high grades, near the pluton) and infiltration of aqueous fluids. Determination of the peak *P–T* conditions and the paths for these various events was carried out using conventional thermobarometry methods such as cation exchange reaction thermometry, multiple equilibria calculations, GASP barometry and petrogenetic grids. Fe–Mg exchange between garnet and biotite thermometers using different calibrations was applied. Solution models of Helffrich & Wood (1989)

https://doi.org/10.1017/S0016756810000841 Published online by Cambridge University Press

Table 4. Activity values used for calculating equilibrium reactions by THERMOCALC

Metamorphic stage	Mineral assemblage	Activity
Peak metamorphic stage	Grt, Bt, Crd, Spl, Pl, Ilm, Opx, Sil, Qtz, H_2O	py – 0.032, alm – 0.35, phl – 0.030, ann – 0.073, east – 0.030, Crd – 0.36, fCrd – 0.18, An – 0.90, Ab – 0.24, Spl – 0.14, herc – 0.85, mt – 0.03768, ilm – 0.62, Opx – 1.00, Sil – 1, Qtz – 1, H_2O – 1

py – pyrope; alm – almandine; ann – annite; phl – phlogopite; east – eastonite; crd – cordierite; fCrd – Fe-cordierite; An – anorthite; Ab – albite; Spl – spinel; herc – hercynite; mt – magnetite; ilm – ilmenite; Opx – orthopyroxene; Sil – sillimanite; Qtz – quartz

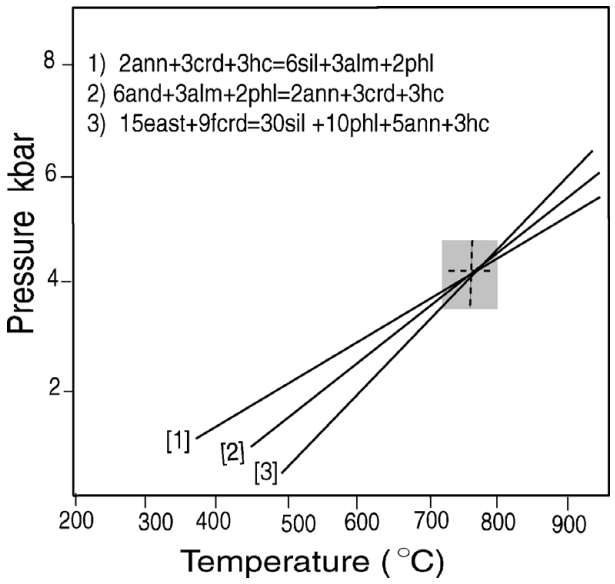

Figure 5. Representative results of multiple equilibria calculation by THERMOCALC (3.2) program; a pressure of ~ 2 kbar and temperature of ~ 750 °C can be considered for peak metamorphism.

and Ganguly & Saxena (1984) were used for garnets. For pressure estimation, GASP (garnet–sillimanite–quartz–plagioclase; Koziol & Newton, 1988) barometers were employed. The outer parts of garnet along with biotites with highest Ti content were used to find the peak temperature, however; plagioclase does not show significant zoning. *P–T* estimation for peak metamorphic paragenesis gives a temperature of 650–700 °C and pressure of 2 kbar. Furthermore, using multiple equilibria (THERMOCALC program version 3.2; Holland & Powell, 1998), temperature and pressure were calculated for the formation of the metapelitic rocks (Fig. 5). Table 4 shows the activity values that were used for calculating equilibrium reactions by THERMOCALC. The results are in good agreement with those from other methods. Activities of biotite, muscovite, garnet and plagioclase end-members were calculated using the AX program of Holland & Powell (1998). On the basis of these data, the studied rocks were at a depth of 6–12 km when they experienced a peak metamorphic temperature. This reflects a mean geothermal gradient of about 58 °C/km, which is in the range of contact aureoles (Spear, 1993). Therefore, peak metamorphism occurred under high-temperature and low-pressure conditions (LP/HT metamorphism) and reflects the high heat flow in this part of the crust. This suggests a genetic link between granite ascent from the deep crust and the high-temperature/low-pressure (contact metamorphism) type of metamorphism in the upper crust.

7. Discussion

The observations in the studied area are consistent with a thermal-tectonic history in which early regional metamorphism (greenschist to amphibolite facies) occurred during initial collision/contraction of continental margin basins and development of a continental margin arc and associated high geothermal gradient. Intermediate stages of contractional history and arc evolution were associated with intrusion of the Alvand Plutonic Complex, including the granite in the Hamadan area that created a low-pressure–high-temperature contact aureole (Sepahi, Whitney & Baharifar, 2004). Therefore, metamorphic rocks of the Hamadan have experienced multiple episodes of metamorphism driven by burial and heating during arc construction and collision, and these events are associated with local partial melting (at high grades, near the pluton).

The metamorphic conditions of the low-grade andalusite-bearing rocks (regional metamorphic rocks) are therefore not well defined by mineral assemblages, but peak temperatures and pressures were likely in the range of 375–500 °C and 2–3 kbar, based on petrogenetic grid considerations, estimates of geothermal gradients, and calculations and inferences for rocks in higher grade zones. For example, garnet–staurolite schist in zone 4 records garnet–biotite Fe–Mg exchange temperatures of 520–570 °C and a pressure of 3 kbar (A. A. Baharifar, unpub. M.Sc. thesis, Tarbiat Moallem Univ. Tehran, Iran, 1997).

The Alvand Plutonic Complex was emplaced at shallow crustal levels and is associated with a low-pressure–high-temperature contact aureole (A. A. Baharifar, unpub. M.Sc. thesis, Tarbiat Moallem Univ. Tehran, Iran, 1997; A. A. Sepahi, unpub. Ph.D. thesis, Tarbiat Moallem Univ. Tehran, Iran, 1999). Cordierite occurs as a texturally late phase near the pluton (< 3 km) in rocks with a hornfels texture, and overprints an earlier andalusite ± sillimanite assemblage. Migmatitic rocks and the assemblages K-feldspar + sillimanite and spinel + plagioclase + cordierite also occur only

https://doi.org/10.1017/S0016756810000841 Published online by Cambridge University Press

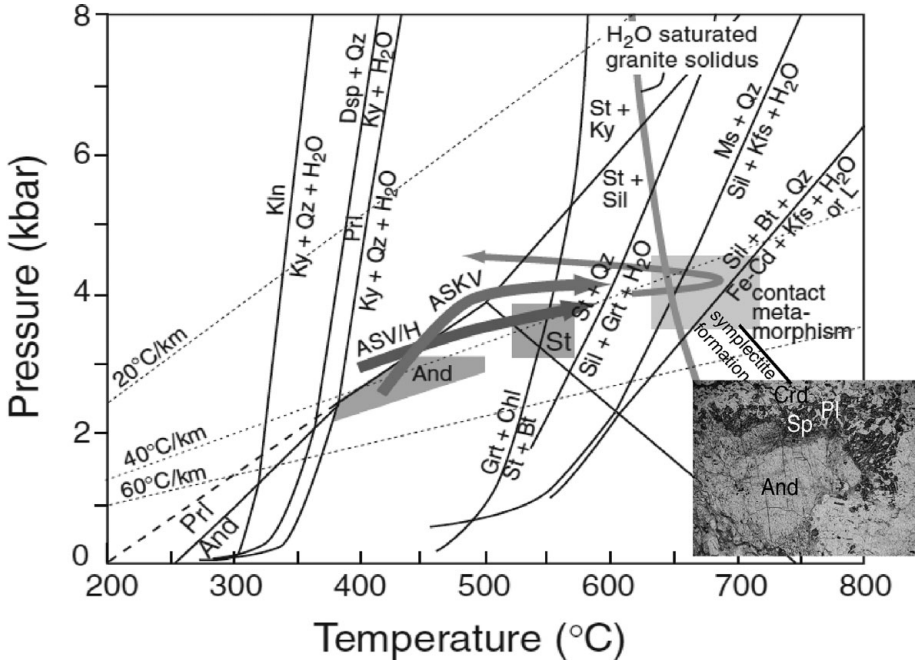

Figure 6. Pressure–temperature diagram (modified after Sepahi, Whitney & Baharifar, 2004) and representative picture of corona evolution in a *P–T* diagram. Al_2SiO_5 triple point from Holdaway (1971); other equilibria calculated using database and software of Berman (1991). *P–T* conditions and paths are shown for selected samples. Dsp – diaspore; Kln – kaolinite; Prl – pyrophyllite. The shaded field labelled 'And' (andalusite) shows the conditions at which the andalusite schists and andalusite–quartz veins may have equilibrated. The field labelled 'St' (staurolite) was calculated for the staurolite–garnet schist (SschH) using garnet–biotite thermometry, brackets from lower and higher grade rocks, and results of Baharifar (1997). The fields labelled 'St + Ky' and 'St + Sil' are partially defined by equilibria (e.g. the upper stability of staurolite + quartz), but the maximum pressure for St + Ky is not known.

near the pluton, implying that the highest temperatures were associated with intrusion of the granite. Mineral assemblages in hornfelsic rocks and the presence of granitic leucosomes suggest that the stability of muscovite in quartz-bearing rocks was exceeded, and that contact metamorphic *P–T* conditions were therefore in excess of 700 °C at moderate to low pressures (~ 4 kbar). Contact metamorphism texturally overprinted regional metamorphic assemblages and fabrics. In some zones near the granite, breakdown of garnet to plagioclase + sillimanite and cordierite is replaced (pseudomorphed) by sillimanite + biotite, implying back reaction of cordierite perhaps during the post-migmatite/granite path that accounts for growth of late kyanite (Sepahi, Whitney & Baharifar, 2004).

The *P–T* diagram (Fig. 6) illustrates the implications of these data. Some rocks (ASKV, ASV, ASVH) record a prograde heating path that is clockwise on a *P–T* diagram. Other rocks that were buried and heated along apparently similar paths to ASV/H, or at slightly higher pressures (kyanite zone), experienced low-pressure–high-temperature contact metamorphism near the Alvand granite, reaching conditions sufficient to break down muscovite and initiate partial melting in pelitic rocks. The contact metamorphosed rocks, the granite itself, and some rocks that are beyond the contact aureole experienced kyanite zone conditions following intrusion of the granite. Whether these rocks were buried and heated (e.g. during contraction associated with collision and suturing) or whether the *P–T* path was dominated by cooling is not defined by our observations, garnet zoning and analyses. The *P–T* diagram, inferred paths and zoning profiles of garnet do not account for the decompression history of the terrane. The breakdown of garnet to plagioclase + sillimanite, dehydration melting and the formation of spinel–plagioclase symplectite on andalusite could occur during decompression or heating; these textures are limited to the contact aureole, so heating is perhaps the more likely explanation for these textures and formation of the symplectites in the metapelitic rocks of the Alvand aureole.

Based on the phases observed in the coronas and on their development between andalusite and matrix (Fig. 2c, d), (exhaustion of the available SiO_2 and/or separation of sillimanite/andalusite from SiO_2-rich matrix domains by cordierite resulted in the formation of localized low-silica activity domains and thus triggered the growth of spinel in the rim of andalusite) and according to the quartz-absent KFMASH reaction, a first-order approximation of the prograde melting reaction is: Sil/And + Bt = Crd + Spl + Kfs + melt.

8. Conclusions

The microstructural and thermobarometric study of this work enabled us to form some conclusions regarding the spinel–cordierite–plagioclase symplectites replacing andalusite in the Hamadan pelites in the Alvand aureole:

(1) The presence of melt shows that spinel–cordierite–plagioclase symplectites replacing andalusite

https://doi.org/10.1017/S0016756810000841 Published online by Cambridge University Press

development occurred under partial melting conditions.

(2) Estimates of the temperature (700 °C) and pressure (~ 2–4 kbar) for the peak metamorphism show that it occurred under LP/HT conditions; the geothermal gradient obtained for the peak metamorphism is 58 °C km^{-1}, which is in the upper range of contact aureole values.

(3) The reaction Sil/And + Bt = Crd + Spl + Kfs + melt is the most common reaction for the development of coronas in the metapelitic rocks of the Alvand aureole.

(4) The *P–T* diagram and inferred paths do not account for the decompression history of the terrane, so breakdown of garnet to plagioclase + sillimanite, dehydration melting and the formation of spinel–plagioclase symplectite are limited to the contact aureole; therefore, heating is perhaps the more likely explanation for formation of the symplectites in the metapelitic rocks of the Alvand aureole.

Acknowledgements. I thank Dr Baharifar for his generous help with electron microprobe analysis. The author is deeply grateful to Dr Mark Allen (Editor of *Geological Magazine*) and two anonymous reviewers for constructive comments.

References

AGARD, P., OMRANI, J., JOLIVER, L. & MOUTHEREAU, F. 2005. Convergence history across Zagros (Iran): constraints from collisional and earlier deformation. *International Journal of Earth Sciences* **94**, 401–19.

AHMADI, A. A., ESMAEILY, D., VALIZADEH, M. V. & RAHIMPOUR-BONAB, H. 2007. Petrology and geochemistry of the granitoid complex of Boroujerd, Sanandaj-Sirjan Zone, Western Iran. *Journal of Asian Earth Sciences* **29**, 859–77.

ALAVI, M. 1994. Tectonics of the Zagros Orogenic belt of Iran: new data and interpretations. *Tectonophysics* **229**, 211–38.

ARVIN, M., PAN, Y., DARGAHI, S., MALEKZADEH, A. & BABAEI, A. 2007. Petrochemistry of the Siah-Kuh granitoid stock southwest of Kerman, Iran: implication for initiation of Neotethys subduction. *Journal of Asian Earth Sciences* **30**, 474–89.

BAHARIFAR, A. A., MOINEVAZIRI, H., BELLON, H. & PIQUE, A. 2004. The crystalline complexes of Hamadan (Sanandaj–Sirjan zone, western Iran): metasedimentary Mesozoic sequences affected by Late Cretaceous tectono-metamorphic and plutonic events, II. ^{40}K–^{40}Ar dating. *Geoscience* **336**, 1443–52.

BERBERIAN, F. & BERBERIAN, M. 1981. Tectono-plutonic episodes in Iran. In *Zagros Hindukush, Himalaya Geodynamic Evolution* (eds H. K. Gupta & F. M. Delany), pp. 5–32. Washington, DC: American Geophysical Union.

BERBERIAN, M. & KING, G. C. 1981. Towards a paleogeography and tectonic evolution of Iran. *Canadian Journal of Earth Sciences* **18**, 210–65.

BERMAN, R. 1991. Thermobarometry using multi-equilibrium calculations: a new technique, with petrological applications. *Canadian Mineralogist* **29**, 833–55.

BUCHER-NURMINEN, K. & DROOP, G. 1983. The metamorphic evolution of garnet–cordierite–sillimanite–gneisses of the Gruf-Complex, Eastern Pennine Alps. *Contributions to Mineralogy and Petrology* **84**, 215–27.

CARSON, C. J., POWELL, R., WILSON, C. J. L. & DIRKS, P. H. G. M. 1997. Partial melting during tectonic exhumation of a granulite terrane: an example from the Larsemann Hills, East Antarctica. *Journal of Metamorphic Geology* **15**, 105–26.

CENKI, B., KRIEGSMAN, L. M. & BRAUN, I. 2002. Melt-producing and melt-consuming reactions in anatectic granulites: P–T evolution of the Achankovil cordierite gneisses, South India. *Journal of Metamorphic Geology* **20**, 543–61.

CESARE, B., MARCHESI, C., HERMANN, J. & GOMEZ-PUNGNAIRE, M. T. 2003. Primary melt inclusions in andalusite from anatectic graphitic metapelites: implications for the position of the Al_2SiO_5 triple point. *Journal of Metamorphic Geology* **31**, 573–6.

CLARKE, G. L. & POWELL, R. 1991. Decompressional coronas and symplectites in granulites of the Musgrave Complex, central Australia. *Journal of Metamorphic Geology* **9**, 441–50.

DROOP, G. T. R. 1989. Reaction history of garnet-sapphirine granulites and conditions of Archaean high-pressure granulite-facies metamorphism in the Central Limpopo Mobile Belt, Zimbabwe. *Journal of Metamorphic Geology* **7**, 383–403.

FAZLNIA, A., SCHENK, V., STRAATEN, F. & MIRMOHAMMADI, M. 2009. Petrology, geochemistry, and geochronology of trondhjemites from the Qori Complex, Neyriz, Iran. *Lithos* **112**, 413–33.

GANGULY, J. & SAXENA, S. 1984. Mixing properties of aluminosilicate garnets: constraints from natural and experimental data and applications to geothermobarometry. *American Mineralogist* **69**, 88–97.

GOLONKA, J. 2004. Plate tectonic evolution of the southern margin of Eurasia in the Mesozoic and Cenozoic. *Tectonophysics* **38**, 235–73.

GRANT, J. A. & FROST, B. R. 1990. Contact metamorphism and partial melting of pelitic rocks in the aureole of the Laramie anorthosite complex, Morton Pass, Wyoming. *American Journal of Science* **290**, 425–72.

GREENFIELD, J. E., CLARKE, G. L. & WHITE, W. 1998. A sequence of partial melting reactions at Mount Stafford, central Australia. *Journal of Metamorphic Geology* **16**, 363–78.

HAND, M., DIRKS, P. H. G. M., POWELL, R. & BUICK, I. S. 1992. How well established is isobaric cooling in Proterozoic orogenic belts? An example from the Arunta inlier, central Australia. *Geology* **20**, 649–52.

HAND, M., SCRIMGEOUR, I., POWELL, R., STÜWE, K. & WILSON, C. J. L. 1994. Metapelitic granulites from Jetty Peninsula, east Antarctica: formation during a single event or by polymetamorphism? *Journal of Metamorphic Geology* **12**, 557–73.

HELFFRICH, G. & WOOD, B. 1989. Subregular model for multicomponent solutions. *American Mineralogist* **74**, 1016–22.

HOLDAWAY, M. J. 1971. Stability of andalusite and the aluminum silicate phase diagram. *American Journal of Science* **271**, 97–131.

HOLLAND, T. J. B. & POWELL, R. 1998. An internally consistent thermodynamic data set for phases of petrological interest. *Journal of Metamorphic Geology* **16**, 309–43.

INGS, S. J. & OWEN, J. V. 2002. Decompressional reaction textures formed by isobaric heating: an example from the thermal aureole of the Taylor Brook Gabbro Complex,

western Newfoundland. *Mineralogical Magazine* **66**, 941–51.

JOHNSON, T., BROWN, M., GIBSON, R. & WING, B. 2004. Spinel–cordierite symplectites replacing andalusite: evidence for melt-assisted diapirism in the Bushveld Complex, South Africa. *Journal of Metamorphic Geology* **22**, 529–45.

KHALAJI, A. A., ESMAEILY, D., VALIZADEH, M. V. & RAHIMPOUR-BONAB, H. 2007. Petrology and geochemistry of the granitoid complex of Boroujerd, Sanandaj-Sirjan Zone, Western Iran. *Journal of Asian Earth Sciences* **29**, 859–77.

KOZIOL, A. M. & NEWTON, R. C. 1988. Redetermination of the anorthite breakdown reaction and improvement of the plagioclase–garnet–aluminosilicate–quartz geobarometer. *American Mineralogist* **73**, 216–23.

KRETZ, R. 1983. Symbols for rock-forming minerals. *American Mineralogy* **68**, 277–9

MARMO, B. A., CLARKE, G. L. & POWELL, R. 2002. Fractionation of bulk rock composition due to porphyroblast growth; effects on eclogite facies mineral equilibria, Pam Peninsula, New Caledonia. *Journal of Metamorphic Geology* **20**, 151–65.

MCDADE, P. & HARLEY, S. L. 2001. A petrogenetic grid for aluminous granulite facies metapelites in the KFMASH system. *Journal of Metamorphic Geology* **19**, 45–59.

MEZGER, J. E., CHACKO, T. & ERDMER, P. 2001. Metamorphism along a late Mesozoic accretionary continental margin: a case study from the northern Coast Belt of the North American Cordillera. *Journal of Metamorphic Geology* **19**, 121–38.

MOHAJJEL, M. & FERGUSSON, C. L. 2000. Dextral transpression in Late Cretaceous continental collision, Sandandaj–Sirjan Zone, western Iran. *Journal of Structural Geology* **22**, 1125–39.

MOHAJJEL, M., FERGUSSON, C. L. & SAHANDI, M. R. 2003. Cretaceous–Tertiary convergence and continental collision, Sanandaj–Sirjan Zone, Western Iran. *Journal of Asian Earth Sciences* **21**, 397–412.

NORLANDER, B. H., WHITNEY, D. L., TEYSSIER, C. & VANDERHAEGHE, O. 2002. Partial melting and decompression of the Thor-Odin Dome, Shuswap metamorphic core complex, Canadian Cordillera. *Lithos* **61**, 103–25.

OMRANI, J., AGARD, PH., WHITECHURCH, H., BENOIT, M., PROUTEAU, G. & JOLIVET, L. 2008. Arc magmatism and subduction history beneath the Zagros Mountains, Iran: a new report of adakites and geodynamic consequences. *Lithos* **106**, 380–98.

PASSCHIER, C. W. & TROUW, R. A. J. 1996. *Microtectonics*. Heidelberg: Springer-Verlag, 289 pp.

PITRA, P. & DE WALL, S. A. 2001. High-temperature, low-pressure metamorphism and development of prograde symplectites, Marble Hall Fragment, Bushveld Complex (South Africa). *Journal of Metamorphic Geology* **19**, 311–25.

RIESCO, M., STÜWE, K., RECHE, J. & MARTINEZ, J. 2004. Silica depleted melting of pelites. Petrogenetic grid and application to the Susqueda Aureole, Spain. *Journal of Metamorphic Geology* **22**, 475–94.

ROBINSON, P. R., HOLLOCHER, K. T., TRACY, R. J. & DIETSCH, C. W. 1982. High grade Acadian regional metamorphism in south-central Massachusetts. In *NEIGC 74th Annual Meeting of the State Geological and Natural History Survey of Connecticut, guidebook for fieldtrips in Connecticut and South-Central Massachusetts* (eds R. A. Joester & S. S. Quarrier), pp. 289–340. Storrs: The University of Connecticut.

SAKI, A. & BAHARIFAR, A. A. 2010. Common melting reactions and their characteristics in the Alvand aureole metapelites, Hamadan. *Iranian Jounal of Geosciences* (in press).

SAKI, A. & POURKASEB, H. 2010. P–T Conditions and fluid composition for wollastonite-clinopyroxene-garnet-bearing calc-silicate rocks from contact aureole of the Alvand batholite, Hamadan. *Shahid Chamran University Journal of Sciences* (in press).

SEARS, J. W., GEORGE, G. M. S. & WINNE, J. C. 2005. Continental rift systems and anorogenic magmatism. *Lithos* **80**, 147–54.

SEDERHOLM, J. J. 1967. *Selected Works: Granite and Migmatites.* Edinburgh: Oliver and Boyd.

SEPAHI, A. A., WHITNEY, D. L. & BAHARIFAR, A. A. 2004. Petrogenesis of And–Ky–Sil veins and host rocks, Sanandaj-Sirjan metamorphic belt, Hamadan, Iran. *Journal of Metamorphic Geology* **22**(2), 119–34.

SHAHABPOUR, J. 2005. Tectonic evolution of the orogenic belt in the region located between Kerman and Neyriz. *Journal of Asian Earth Sciences* **24**, 405–17.

SHAHBAZI, H., SIEBEL, W., POURMOAFEE, M., GHORBANI, M., SEPAHI, A. A., SHANG, C. K., VOUSOUGHI. & ABEDINI, M. 2010. Geochemistry and U–Pb zircon geochronology of the Alvand plutonic complex in Sanandaj–Sirjan Zone (Iran): new evidence for Jurassic magmatism. *Journal of Asian Earth Sciences*, doi:10.1016/j.jseaes.2010.04.014, in press.

SPEAR, F. S. 1993. *Metamorphic Phase Equilibria and Pressure–Temperature–Time Paths*. Monograph 1. Washington, DC: Mineralogical Society of America.

STÜWE, K. 1997. Effective bulk composition changes due to cooling: a model predicting complexities in retrograde reaction textures. *Contributions to Mineralogy and Petrology* **129**, 43–52.

TOPUZ, G., ALTHERRA, R., KALTA, A., SATIRB, M., WERNERA, O. & SCHWARZA, W. H. 2004. Aluminous granulites from the Pulur complex, NE Turkey: a case of partial melting, efficient melt extraction and crystallisation. *Lithos* **72**, 183–207.

VERNON, R. H. 1996. Problems with inferring P–T–t paths in low-P granulite facies rocks. *Journal of Metamorphic Geology* **14**, 143–53.

WATERS, D. J. 1991. Hercynite-quartz granulites: phase relations and implications for crustal processes. *European Journal of Mineralogy* **3**, 367–86.

WHITE, R. W., POWELL, R. & CLARKE, G. L. 2002. The interpretation of reaction textures in Fe-rich metapelitic granulites of the Musgrave Block, central Australia: constraints from mineral equilibria calculations in the system K_2O–FeO–$MgOAl_2O_3$–SiO_2–H_2O–TiO_2–Fe_2O_3. *Journal of Metamorphic Geology* **20**, 41–55.

WHITE, R. W., POWELL, R. & CLARKE, G. L. 2003. Prograde metamorphic assemblage evolution during partial melting of metasedimentary rocks at low pressures: migmatites from Mt Stafford, Central Australia. *Journal of Petrology* **44**, 1937–60.

WHITE, R. W., POWELL, R. & HOLLAND, T. J. B. 2001. Calculation of partial melting equilibria in the system Na_2O–CaO–K_2O–FeO–MgO–Al_2O_3–SiO_2–H_2O (NCKFMASH). *Journal of Metamorphic Geology* **19**, 139–53.

WHITTINGTON, A., HARRIS, N. & BAKER, J. 1998. Low-pressure crustal anatexis. In *What Drives Metamorphism and Metamorphic Reactions?* (eds P. J. Treolar & P. J. O'Brien), pp. 183–98. Geological Society of London, Special Publication no. 138.